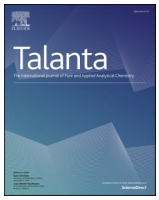
Talanta 295 (2025) 128411



Contents lists available at ScienceDirect

Talanta

journal homepage: www.elsevier.com/locate/talanta



# AND logic gate-based alternating PER-Cas12a signal amplification system for ultrasensitive detection of sEVs

Man Wang, XuZhen Zhang, Jiayi Fan, Cuiling Zhang *, Yuezhong Xian **

*School of Chemistry and Molecular Engineering, East China Normal University, 500 Dongchuan Road, Shanghai, 200241, PR China*

ARTICLE INFO

*Keywords:*
Small extracellular vesicles (sEVs)
Alternating primer exchange reaction (Alt-PER)
CRISPR-Cas12a
Dual-protein recognition
Breast cancer

ABSTRACT

Protein biomarkers on breast cancer-derived small extracellular vesicles (BC-sEVs) hold great promise in liquid biopsy. However, it remains challenging due to their inherent heterogeneity and low abundance. Herein, we developed an AND logic gate-based DNA cascade signal amplification strategy, termed Alternating Primer Exchange Reaction-activated Cas12a (Alt-PER-Cas12a), for the ultrasensitive detection of BC-sEVs in clinic samples. This dual-protein recognition system employs EpCAM/MUC1-specific capture probes to release two DNA hairpins (Hep and Hmu) as AND gate inputs in Alt-PER. The corresponding Hep and Hmu hairpins can initiate the Alt-PER with a large amount of primers to generate long single-stranded DNA products with alternating repeat units. Each repeating unit serves as a CRISPR activator, inducing the *trans*-cleavage activity of Cas12a and enabling cascade signal amplification. The as-constructed strategy exhibits excellent sensitivity with LOD of 2.6 $\times$ $10^3$ particles/mL. It has been successfully used to discriminate breast cancer patients from healthy donors (AUC = 0.992) in clinical validation, and shows great potential for liquid biopsy.

## 1. Introduction

Breast cancer has become the most prevalent malignancy among women, with its incidence continuing to rise steadily [1–4]. While tissue biopsy remains the clinical gold standard for breast cancer diagnosis, its invasive nature poses significant challenges, including an increased risk of recurrence and metastasis, susceptibility to sampling bias, and the inability to provide real-time monitoring of tumor progression. Moreover, the procedure itself may adversely affect patient survival and prognosis [5–8]. Liquid biopsy has emerged as a highly promising alternative, offering advantages such as minimal invasiveness, cost-effectiveness, and ease of sample collection [9,10]. Among the various liquid biopsy markers, small extracellular vesicles (sEVs) secreted by cells with nanoscale size (30–200 nm in diameter) enclosed by a lipid bilayer are particularly attractive due to their widespread distribution in bodily fluids and exceptional stability in circulation system [11–13]. sEVs carry some key biomolecules that reflect the molecular signatures of their parent cells [14]. It was also reported that tumor cells could secrete up to 10 times more sEVs than normal cells [15,16]. The characteristic enables the detection of cancer-specific biomarkers even before clinical symptoms manifest, providing crucial opportunities for early diagnosis and therapeutic intervention [14]. Consequently, sEVs have attracted attention as non-invasive, reliable biomarkers for liquid biopsy-based cancer diagnostics [17–19].

In the early stages of cancer, tumor-derived sEVs in blood are present at low concentrations and heterogeneity. These pose significant challenges for highly sensitive sEVs detection. To enhance detection sensitivity, various signal amplification strategies were developed, including rolling circle amplification (RCA) [20,21], primer exchange reaction (PER) [22,23], hybridization chain reaction (HCR) [24,25], toehold-mediated strand displacement (TMSD) [26], and CRISPR/Cas systems [27]. The primer exchange reaction (PER) can append special sequence domains to primers [28]. This programmable amplification strategy has been successfully applied in biosensing and cellular bioimaging [29–33]. The key advantages of PER lie in its simplicity, requiring only three core components of a DNA polymerase, primer DNA, and hairpin DNA. This system allows for sequence design based on Boolean logic operations to achieve efficient amplification [28,34,35]. The CRISPR-Cas system, a powerful RNA-guided gene-editing technology, has been widely applied for molecular diagnostics [36–38]. In the CRISPR-Cas12a system upon crRNA-target DNA hybridization, Cas12a exhibits dual functionality of precise cleavage of double-stranded DNA

* Corresponding author.
** Corresponding author.
*E-mail addresses:* clzhang@chem.ecnu.edu.cn (C. Zhang), yzxian@chem.ecnu.edu.cn (Y. Xian).

https://doi.org/10.1016/j.talanta.2025.128411
Received 6 April 2025; Received in revised form 13 May 2025; Accepted 27 May 2025
Available online 27 May 2025
0039-9140/© 2025 Published by Elsevier B.V.

and robust *trans*-cleavage activity against single-stranded DNA [39–42]. This unique dual-functionality endows CRISPR-Cas12a with exceptional signal amplification capacity for molecular diagnostics [43–46]. However, these methods exhibit inherent limitations in efficiency and generalizability. Given the programmability of DNA reactions, cascading signal amplification strategies can significantly enhance the performance of biosensing system [47–49].

In addition to sensitivity, heterogeneity is an important issue for sEVs detection [50,51]. Studies have shown that simultaneous analysis of multiple biomarkers can significantly solve the false positives from heterogeneity, thereby improving the accuracy of diagnosis [52]. Researchers have developed some detection systems based on DNA logic devices capable of processing multiple signal inputs and generating defined output through Boolean operation [53,54]. Compared to conventional single protein detection strategies, DNA logic circuits incorporating "AND" logic operations offer improved specificity through effective reduce the interference of phenotypic heterogeneity [55–57].

Systematic evolution of ligands by exponential enrichment yields DNA aptamers with high specificity and strong binding affinity for various biomarkers, including surface proteins on sEVs [58–60]. Upon target binding, these aptamers undergo conformational changes, releasing pre-hybridized complementary DNA strands. This structure-switching aptamer mechanism effectively converts sEVs surface protein information into detectable DNA signals [61–65]. Importantly, when these DNA signals are incorporated into AND logic gate systems, they enable simultaneous analysis of multiple surface biomarkers on sEVs, thereby significant enhancement the accuracy of cancer diagnostics.

We herein developed an AND logic gate-based DNA cascade signal amplification system, termed Alternating Primer Exchange Reaction-activated Cas12a (Alt-PER-Cas12a), for the ultrasensitive recognition dual-protein biomarkers on the surface of breast cancer-derived sEVs. EpCAM and MUC1 proteins, overexpressed on breast cancer-derived sEVs, were selected as model targets. As illustrated in Fig. 1, we employed two types of magnetic capture probes (EpCAM and MUC1 aptamers along with their complementary hairpin DNA (Hep and Hmu)). Due to the coexistence of EpCAM and MUC1 on breast cancer-derived sEVs, the two aptamers specifically bind to their targets, and trigger the simultaneous release of Hep and Hmu hairpins as AND logic gate inputs. Upon the addition of excess primer P, these few hairpins initiate a self-sustaining primer exchange reaction, wherein primer P alternately extends along Hep and Hmu templates, generating abundant alternating repeat products. These repetitive units consist of multiple tandem sequences that are complementary to the crRNA guide region. Upon hybridization with the Cas12a-crRNA complex, they form an active ternary structure, inducing conformational changes in Cas12a to expose its catalytic domain. The activated Cas12a exhibits nonspecific *trans*-cleavage activity, indiscriminately digesting nearby single-stranded DNA (FQ reporter probes). This cascade amplification results in a substantial and robust fluorescence signal, enabling the ultrasensitive detection of sEVs based on dual-protein recognition. The proposed strategy holds great promise for precise sEVs detection and liquid biopsy.

## 2. Experimental section

### 2.1. Native PAGE analysis

All DNA oligonucleotides were dissolved in 1 × TE buffer and diluted to 10 μM in PBS, followed by annealing at 95 °C for 5 min and gradual cooling to room temperature over 1 h. The amplification reaction system contained 500 nM each of hairpin Hep, hairpin Hmu, and primer P in 1 × PBS buffer supplemented with 0.8 U/μL Bst DNA polymerase (large fragment), 10 mM $MgSO_4$, 1 × ThermoPol buffer, and dNTP mixture (900 μM each of dATP, dTTP, and dCTP). The Alt-PER reaction was performed at 37 °C for 90 min. For PAGE analysis, 10 μL of samples were mixed with 2 μL of 6 × DNA loading buffer and electrophoresed on 12 % polyacrylamide gels at 110 V for 90 min, followed by Gel-Red staining

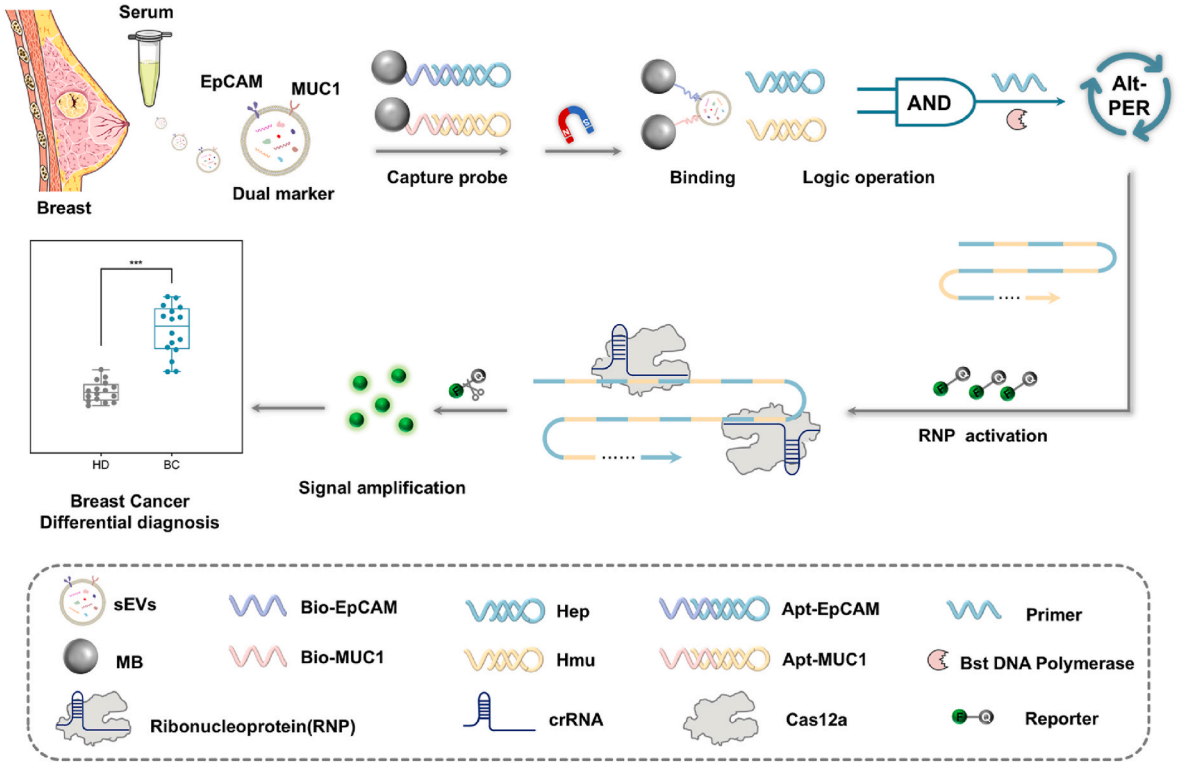



**Fig. 1.** Schematic diagram of dual-aptamer assisted AND logic gate driven Alt-PER-Cas12a cascade signal amplification for sensitive sEVs detection and breast cancer identification.

and imaging. To validate the responsiveness, capture probes were incubated with sEVs, magnetically separated, and the supernatant was analyzed by PAGE (60 min electrophoresis) using identical procedures.

### 2.2. Validation performance of and logic gate

We established a binary logic system based on hairpin DNAs (Hep and Hmu) and verified its functionality through four input combinations, including (00) no hairpins, (10) Hep only, (01) Hmu only, and (11) both Hep and Hmu. The reaction system, consisting of 5 nM hairpins (Hep/Hmu) and 400 nM primer P in Alt-PER amplification buffer, was incubated at 37 °C for 90 min and inactivated at 80 °C for 20 min. For Cas12a activation, 5 μL of Alt-PER products were added to a detection system containing 30 nM Cas12a, 30 nM crRNA, 1 × NEBuffer r2.1, 0.5 μM FQ reporter) in 384-well plates, and the fluorescence signal was measured every 1 min at 37 °C. To assess amplification efficiency, parallel experiments were conducted using 5 nM target sequence (TS) in the Cas12a-crRNA system under the same conditions.

### 2.3. Characterization of sEVs

TEM analysis of MCF-7-sEVs was performed by adsorbing 10 μL of samples onto copper grids for 15 min, followed by negative staining with 1 % uranyl acetate for 2 min and subsequent washing before imaging. For NTA, sEVs were diluted 400 × in PBS to assess the size distribution and determine the concentration.

### 2.4. Preparation of capturing probes

The Bio-EpCAM and hairpin Hep were mixed with a concentration of 10 and 15 μM in PBS, respectively. Then, the mixture was denatured at 95 °C for 5 min, and gradually cooled to room temperature, forming the Apt-EpCAM hybrid complex. The Apt-MUC1 complex was prepared using the same procedure with Bio-MUC1 and hairpin Hmu. For probe preparation, 50 μL of streptavidin-coated magnetic beads (SA-MBs, 10 mg/mL) were washed three times with 500 μL of Buffer I (10 mM Tris-HCl, pH 7.5; 1 M NaCl; 1 mM EDTA; 0.05 % Tween-20). The washed beads were incubated with 50 μL Apt-EpCAM hybrid and 450 μL of Buffer II (10 mM Tris-HCl, pH 7.5; 1 M NaCl; 1 mM EDTA) under a rotary mixer at room temperature for 1 h. After incubation, the supernatant was collected for UV absorption analysis to assess conjugation efficiency. The Apt-EpCAM-conjugated beads (MB1) were washed three times with Buffer I and once with PBS, then resuspended in PBS at 2 mg/mL for storage at 4 °C. The MUC1-specific probe (MB2) was prepared following the same protocol.

### 2.5. Alt-PER-Cas12a system for sEVs detection

2.5 μL each of Apt-EpCAM-conjugated MB1 and Apt-MUC1-conjugated MB2 were added to diluted sEVs solutions. The samples were incubated on a rotary mixer at room temperature for 1 h to release target-specific hairpins (Hep and Hmu). After magnetic separation, the supernatant was collected and transferred to a system containing 400 nM primer P in 1 × PBS supplemented with 0.8 U/μL Bst DNA polymerase (large fragment), 10 mM $MgSO_4$, 1 × ThermoPol buffer, and dNTP mixture (dATP/dTTP/dCTP). Alt-PER reactions were conducted at 37 °C for 90 min and terminated by heat inactivation at 80 °C for 20 min. For signal detection, 5 μL of Alt-PER products were added to a CRISPR-Cas12a detection system containing 30 nM Cas12a, 30 nM crRNA, 1 × NEBuffer r2.1, and 0.5 μM FQ reporter probe in 384-well plates. Fluorescence intensity at 523 nm (λex = 488 nm) was measured at 1min interval using a multimode plate reader.

### 2.6. Clinical sample detection

For clinical validation, 32 serum samples were collected from the affiliated YiXing Hospital of Jiangsu University. Samples were homogenized by gentle pipetting and sequentially centrifuged at 2000×*g* for 10 min (4 °C) to remove cellular debris, followed by 10,000×*g* for 30 min at 4 °C to eliminate free proteins. The clarified serum supernatants were aliquoted and stored at −80 °C. sEVs detection in clinical serum samples followed the same workflow as that used for cell culture-derived sEVs, ensuring methodological consistency.

## 3. Results and discussion

### 3.1. Design principle of the and logic gate-based Alt-PER system

The Alt-PER system served as the input module for AND logic gating and the cascade signal amplification was schematically shown in Fig. S1. Through rational primer design, the Alt-PER process can be initiated when primer P hybridizes via its domain to the *a** region of hairpin Hep, which enables Bst polymerase to extend along the Hep template and generate an *a-b* product. Upon reaching the terminator sequence, the extended strand dissociates, and free Hep template to recruit primer P molecules for continuous PER cycles. In the presence of hairpin Hmu, the b segment of the *a-b* product serves as a secondary primer by binding to the complementary *b** region of Hmu, facilitating further extension into an *a-b-a* repeat sequence. This regenerated domain can then be reinitiated on the Hep template, establishing an autonomous amplification loop that progressively elongates the DNA product. The alternative templating between Hep and Hmu yields long single-stranded DNA (ssDNA) with periodic *b-a* repeats, and each repeat unit maintains the capacity to initiate subsequent rounds of amplification while preserving the original template structures. Theoretically, this system enables continuous generation of unlimited *b-a* alternating ssDNA products by employing hairpins Hep and Hmu as templates, provided sufficient Bst DNA polymerase, dNTPs, primers, and reaction time. This target-conserving, self-perpetuating cyclic amplification enables exponential signal amplification while preserving the original biomarker templates throughout the reaction.

The initial *a-b* product generated by PER remains inactive for Cas12a activation due to its incomplete complementarity with crRNA. However, in presence of both hairpins (Hep and Hmu), the alternating PER reactions produce *a-b-a* sequences, wherein the *b-a* segment achieves perfect crRNA complementarity. This specific recognition triggers the *trans*-cleavage activity of Cas12a, leading to the degradation of the FQ reporter probe and the subsequent release of fluorescent signals. This process establishes a secondary amplification that greatly improves detection sensitivity.

### 3.2. Validation the performance of and logic gate

Fig. 1A shows the dual-hairpin induced AND logic gate for surface protein recognition and subsequent Alt-PER signal amplification. Polyacrylamide gel electrophoresis (PAGE) analysis of Alt-PER products confirmed the generation of elongated DNA strands (Fig. 2B). Control lanes in PAGE demonstrated the co-migration of unreacted Hep and Hmu hairpins in absence of primer P (Lane 1, intensified band at hairpin position) and the unextended primer P in the absence of templates (Lane 2). Lane 3 showed the selective extension in single-hairpin system with the conversion of primer P into an *a-b* product (intermediate mobility) with an intact Hep template, whereas Lane 4 maintained unmodified P and Hmu due to the lack of a compatible initiation site. Critically, the complete reaction system (Lane 5) exhibited full primer consumption and production of a series of high molecular weight DNA species, exceeding the size of individual hairpins while preserving their templates. It demonstrates AND-gate-dependent generation of alternating *b-a* repeat sequence through processive primer extension. These results establish the essential dual-input requirement for effective Alt-PER amplification.

To verify the feasibility of AND-gate, we evaluated all four binary

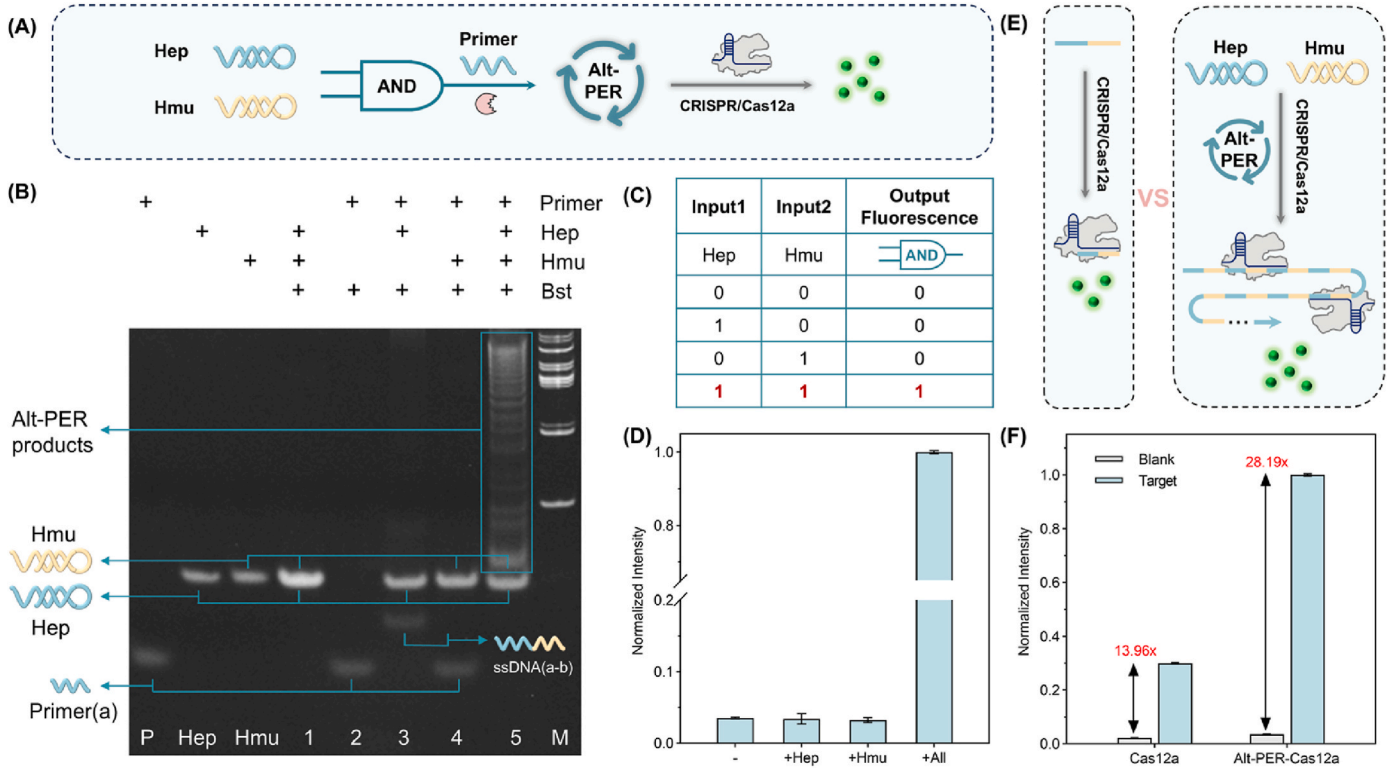



**Fig. 2.** (A) Schematic diagram for the validation the feasibility of AND logic gate through Alt-PER-Cas12a signal amplification. (B) PAGE analysis of Alt-PER products. (C) Truth table of the AND logic gate. (D) Fluorescence intensity output of FAM for the four input combinations (00, 10, 01, 11), respectively. (E) Schematic demonstration of signal amplification through conventional Cas12a system and the Alt-PER-Cas12a system. (F) Fluorescence intensity of Cas12a reactions triggered by equal concentrations of TS and hairpin DNA. The Cas12a reaction was performed with 30 nM Cas12a-crRNA, 5 nM TS and the Alt-PER-Cas12a reaction was conducted in PER buffer containing 30 nM Cas12a-crRNA, 400 nM P, 5 nM Hep, and 5 nM Hmu. Blank represents the fluorescence intensity in the absence of TS or hairpin DNA.

input states (00, 10, 01, 11), as illustrated in the truth table (Fig. 2C), enabling a quantitative assessment of hairpin cooperativity in signal amplification. Fluorescence analysis (Fig. 2D) showed negligible signal output in three control conditions of no hairpins (−), Hep-only (+Hep), and Hmu-only (+Hmu), which was consistent with the inability to generate crRNA-complementary sequences. Only the simultaneous presence of both hairpins (+All) triggered a significant fluorescence signal. It confirmed Alt-PER successfully produced *b-a* repeat sequence for efficient Cas12a activation. These results demonstrate perfect Boolean logic correspondence, where only the "11″ input (Hep + Hmu) yields a TRUE logic output, whereas all other states ("00″, "10″, and "01″) remain FALSE, thereby validating the dual-input requirement for Alt-PER driven amplification.

To quantitatively assess the contributions of hairpins Hep and Hmu for signal amplification and detection sensitivity, we compared the performance of Alt-PER-Cas12a system with that of conventional Cas12a (Fig. 2F). The traditional Cas12a system exhibited 14-fold fluorescence enhancement over blank controls, whereas the Alt-PER-Cas12a system achieved 28-fold higher signal intensity, representing 100 % improvement. This enhanced performance is attributed to two key reasons that (1) the non-consumptive nature of hairpin templates (Hep/Hmu) permits their reuse for sustained amplification cycles under optimal conditions, and (2) the AlterPER reaction produces long ssDNA products containing multiple activator repeats (*b-a* units) capable of independent triggering Cas12a *trans*-cleavage for cascaded signal multiplication. This reveals that the Alt-PER-Cas12a can be employed for ultrasensitive target detection.

### 3.3. Characterizations of sEVs

We extracted sEVs from the MCF-7 breast cancer cells and characterized them by transmission electron microscopy (TEM) and nanoparticle tracking analysis (NTA) analysis. As shown in Fig. 3, TEM image displayed sEVs with characteristic cup-shaped morphology and the size was about 100 nm. NTA measurement demonstrated the hydrodynamic diameter of sEVs approximately 141 nm and concentration about $1.7 \times 10^{11}$ particles/mL. The observed size discrepancy (NTA > TEM) reflects inherent methodological difference. NTA measures the hydrated particle diameter, including the solvation shell, whereas TEM assesses dehydrated dimensions under vacuum, thereby confirming the successful extraction of sEVs.

### 3.4. Construction of sEV-Responsive capture probes

Fig. 4A shows the schematic illustration of the response of capture probes toward sEVs. Two kinds of magnetic capture probes were prepared, and separately incubated with sEVs at room temperature for 1 h. The supernatant was collected via magnetic separation for subsequent experiments to validate the responsiveness of the capture probes toward sEVs.

The successful conjugation of the DNA probes to magnetic beads (MBs) was confirmed through ultraviolet–visible (UV–Vis) absorption spectroscopy. As shown in Fig. 4B, a sharp decrease in absorbance at 260 nm was observed in the supernatant after incubating the biotinylated aptamer-hairpin DNA hybrid complexes with streptavidin-coated magnetic beads, whereas the non-biotinylated hybrid complexes showed no notable change in absorbance under the same incubation conditions (Fig. S2A). Furthermore, the modification of hybrid complexes resulted in more negatively charged bead surface (Fig. S2B). This indicating efficient immobilization of the DNA sequences onto the bead surfaces.

PAGE confirmed both the successful assembly of aptamer-probe

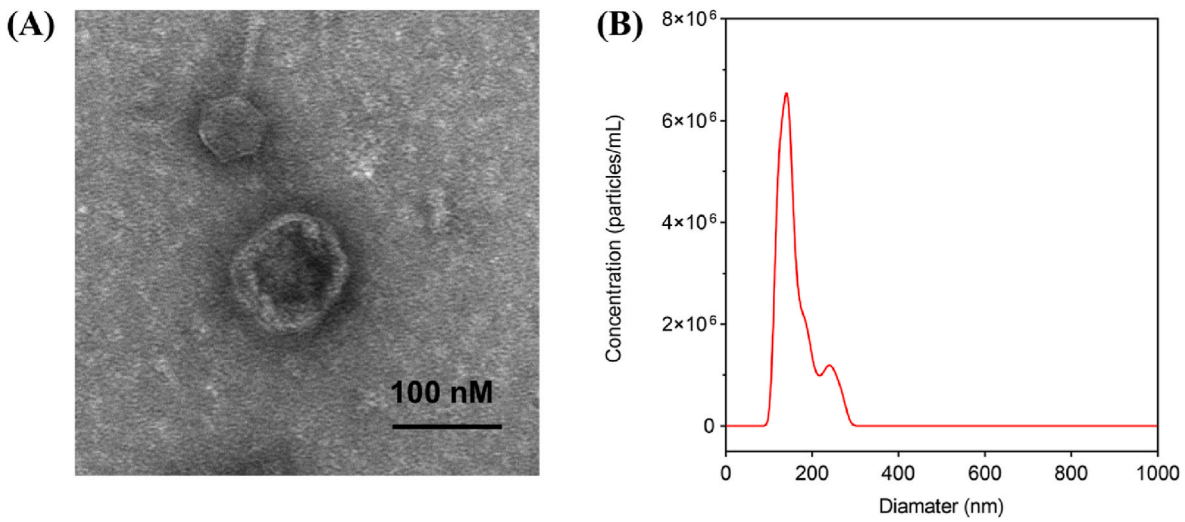



**Fig. 3.** (A) TEM image of the sEVs from MCF-7 cells. (B) NTA detection of sEVs concentration and size distribution.

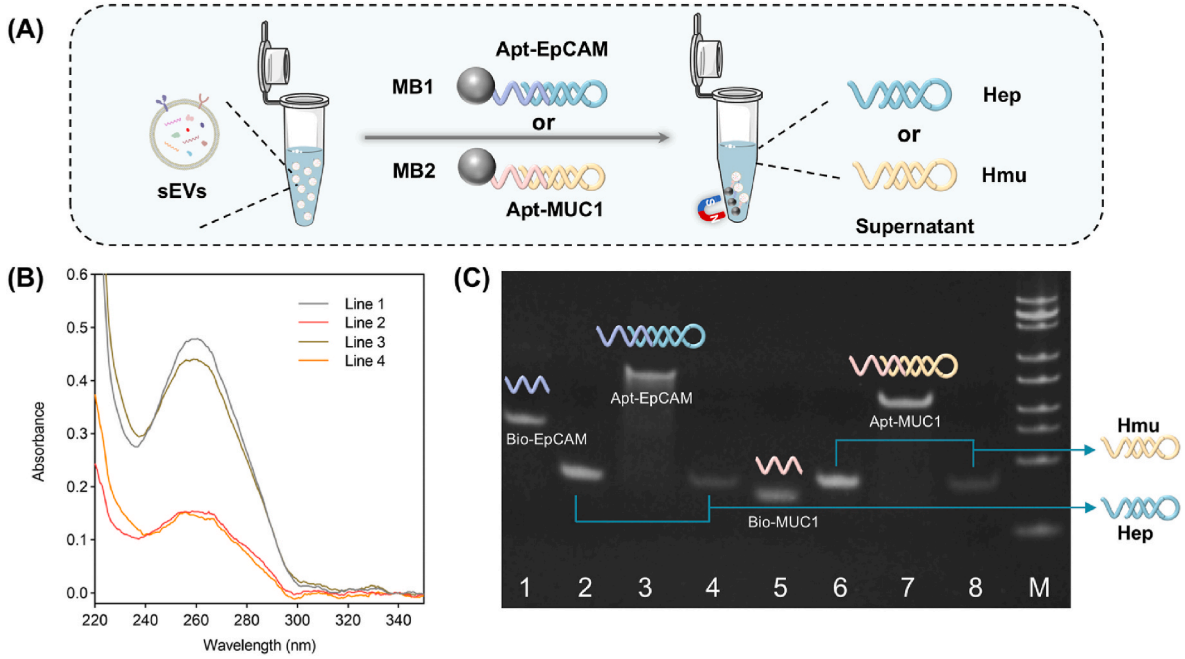



**Fig. 4.** (A) Schematic illustration of the response of capture probes toward sEVs. (B) UV–vis absorption spectra of biotin-modified hybrid complexes in the supernatant before (Line 1, Line 3) and after (Line 2, Line 4) incubation of the corresponding hybrid complexes with MBs. Line 1: Apt-EpCAM; Line 2: Apt-EpCAM + MBs; Line 3: Apt-MUC1; Line 4: Apt-MUC1 + MBs. (C) Results of PAGE analysis. Lane 1, Bio-EpCAM; Lane 2, Hep; Lane 3, Apt-EpCAM; Lane 4, supernatant of sEVs incubated with MB1; Lane 5, Bio-MUC1; Lane 6, Hmu; Lane 7, Apt-MUC1; Lane 8, supernatant of sEVs incubated with MB2; Lane M, DNA molecular weight marker.

complexes and their target-responsive functionality (Fig. 4C). In lane 3, a distinct band with slower migration compared to the individual biotinylated EpCAM (Bio-EpCAM) or Hep components verified the formation of Aptamer-EpCAM heteroduplex. Similarly, lane 7 exhibited a higher molecular weight band than these of biotinylated MUC1 (Bio-MUC1) or Hmu controls, confirming the successful assembly of Apt-MUC1. After incubation of sEVs with capture probe MB1 and subsequent magnetic separation, PAGE analysis of the supernatant (lane 4) exhibited a discrete band aligning with the Hep reference, demonstrating the specific recognition of EpCAM on the surface of sEVs by MB1, and the conformation-induced aptamer switching releases Hep hairpin. Parallel experiments with MB2 (lane 8) showed similar release behavior of Hmu upon MUC1 engagement, thereby confirming the general responsiveness of both probes. Furthermore, dynamic light scattering (DLS) analysis revealed a significant increase in the average hydrodynamic diameter of the MBs following sEVs capture (Fig. S3).

### 3.5. *Optimization of experimental parameters*

To achieve optimal detection performance, we systematically evaluated four key parameters, including the concentration of capture probes, Bst polymerase, primer and the Alt-PER reaction time. As shown in Fig. S4A, a 1:1 mixture of MB1 and MB2 capture probes showed signal saturation at 0.5 mg/mL, and higher concentrations led to the increasing of background noise. Fig. S4B demonstrated the changes of signal over the concentration range of Bst polymerase (0.4–1.2 U/μL). It could be observed that the value of $(F–F_0)/F_0$ did not improve significantly beyond 0.8 U/μL. Thus, it was selected as the optimal concentration for

the following experiments. Fig. S4C and S4D indicated that a primer concentration of 400 nM for 90 min reaction yielded maximum signal. Consequently, the optimal conditions were 0.5 mg/mL capture probes, 0.8 U/μL Bst polymerase, 400 nM primer for 90 min Alt-PER reaction.

### 3.6. Detection of sEVs

We implemented an integrated capture probe and AND logic gate-based Alt-PER-Cas12a system for MCF-7-derived sEVs detection. Fluorescence measurements in Fig. 5A revealed negligible signal in negative controls, including probe-free (column a) and single-probe system (columns b and c), respectively. Detectable background signal was observed in probe-only condition (without sEVs, column d) might be attributed to the mechanical disruption of magnetic handling. Excellent signal amplification was realized in the system containing probes and sEVs (column e), achieving a 3.8-fold enhancement over background ($p < 0.001$), thereby confirming the robust specificity in target detection.

Fig. 5B showed the time-dependent fluorescence kinetics for different concentrations of sEVs within 120 min. An excellent linear correlation ($R^2 = 0.9958$) was obtained between the fluorescence intensity and logarithmic concentration of sEVs over a broad dynamic range of $3.4 \times 10^3$-$1.7 \times 10^7$ particles/mL (Fig. 5C). The regression equation was $F = 3395 \times lgC - 6929$, and the limit of detection was calculated as $2.6 \times 10^3$ particles/mL by 3σ criterion. Compared with the PER- or CRISPR-based technologies for sEVs detection (Table S2), the Alt-PER-CRISPR system employs Alt-PER as a signal input to construct an AND logic gate, enabling dual-protein detection while enhancing sensitivity through a cascaded signal amplification. The system showed comparative or superior performance relative to other AND logic gate-based methods (Table S3). The results revealed that we successfully developed a highly sensitive detection of tumor-derived sEVs approach.

To further validate the target-specific detection capability of the Alt-PER-Cas12a system, we analyzed sEVs derived from non-tumorigenic human mammary epithelial MCF-10A cells (Fig. S5). Fluorescence measurements revealed that the signal intensity for MCF-7-derived sEVs (EpCAM+, MUC1+) was significantly higher than that of MCF-10A-derived sEVs (EpCAM-, MUC1-), while the signal from MCF-10A sEVs remained comparable to the blank control group (Fig. S6). These results confirm the high specificity of the system toward target sEVs.

### 3.7. Clinical sample analysis

We further assessed the anti-interference of the Alt-PER-Cas12a system in a complex matrix, with 10 % and 30 % FBS. While there were slight increases in the standard deviation (SD) values under both 10 % and 30 % FBS conditions, the fluorescence intensities remained remarkably stable and did not display any significant differences compared to the control (Fig. 6A). This confirms the potential clinical applicability for sEVs detection in complex biological systems.

To evaluate the applicability of the AND logic gate-based Alt-PER-Cas12a method in clinical samples, we analyzed serum samples (Table S4) from 16 breast cancer (BC) patients and 16 healthy donors (HD) based on the as-constructed system. As shown in Fig. 6B, the BC group exhibited significantly higher fluorescence signals than that of HD group ($P < 0.001$ by *t*-test), indicating elevated expression of EpCAM and MUC1 proteins on sEVs surfaces in breast cancer patients. Receiver operating characteristic (ROC) curve analysis in Fig. 6C demonstrated excellent diagnostic performance with an AUC (the area under the ROC curve) of 0.992, which can effectively distinguish BC patients from healthy individuals. The heatmap in Fig. 6D further confirmed breast cancer-specific fluorescence signature with relative strong intensity gradient, providing intuitive differentiation between healthy donors and breast cancer patients.

## 4. Conclusions

We design an AND logic gate system that employs dual hairpin DNA inputs to drive cascade signal amplification through the combination of Alt-PER with CRISPR-Cas12a (Alt-PER-Cas12a). For detection sEVs through simultaneous recognition dual-positive proteins (EpCAM and MUC1) on surfaces, the system operates via target-specific aptamer binding, which competitively releases two hairpin DNA as templates for Alt-PER. The Alt-PER reaction programmatically generates long single-stranded DNA products with alternating repeat units via a target-conserving, self-sustaining cycle through the coordinated action of both hairpins. Each repeat unit efficiently activates *trans*-cleavage activity of Cas12a, enabling cascade signal amplification for ultrasensitive detection of breast cancer cell-derived sEVs with LOD of $2.6 \times 10^3$ particles/mL. Clinical sample test demonstrated high diagnostic accuracy (AUC = 0.992), which can statistically distinguish breast cancer patients from healthy donors. The modular Alt-PER design allows flexible detection different targets through the modification of hairpin sequences, and shows great potential for disease diagnostic based on precise identification surface biomarkers on sEVs.

## CRediT authorship contribution statement

**Man Wang:** Writing – original draft, Methodology, Conceptualization. **XuZhen Zhang:** Methodology, Data curation. **Jiayi Fan:** Visualization, Data curation. **Cuiling Zhang:** Writing – review & editing,

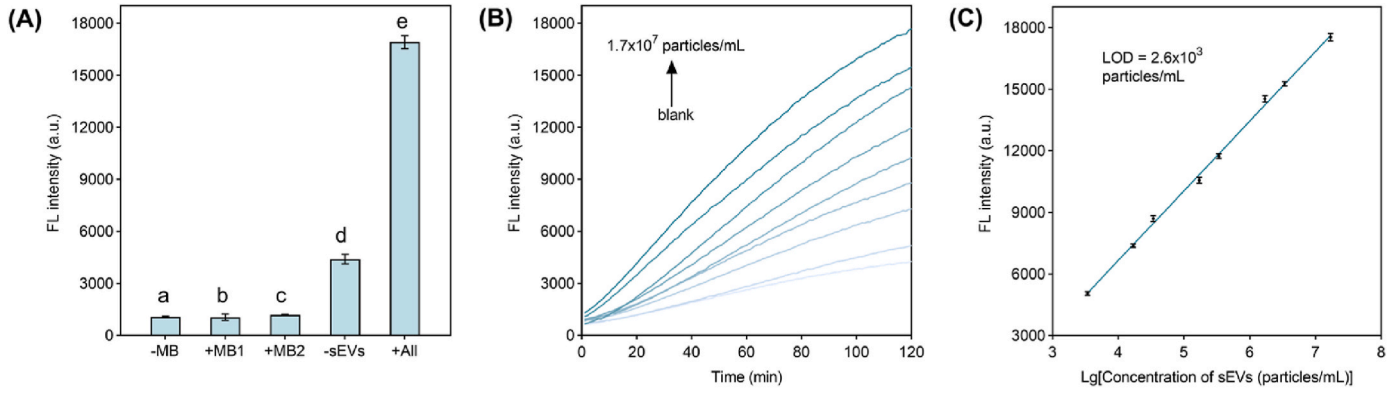



**Fig. 5.** (A) Fluorescence intensity of Alt-PER-Cas12a system under different conditions. a. sEVs; b. sEVs + MB1; c. sEVs + MB2; d. MB1+MB2; e. sEVs + MB1+MB2. The concentration of sEVs was about $1.7 \times 10^7$ particles/mL. (B) The changes of fluorescence intensity over time for the detection of sEVs with different concentrations using the Alt-PER-Cas12a system driven by an AND logic gate. The concentration of sEVs were 0, $3.4 \times 10^3$, $1.7 \times 10^4$, $3.4 \times 10^4$, $1.7 \times 10^5$, $3.4 \times 10^5$, $1.7 \times 10^6$, $3.4 \times 10^6$ and $1.7 \times 10^7$ particles/mL, respectively. (C) The linear relationship between fluorescence intensity and the logarithm of the sEVs concentration over the range of $3.4 \times 10^3$-$1.7 \times 10^7$ particles/mL.

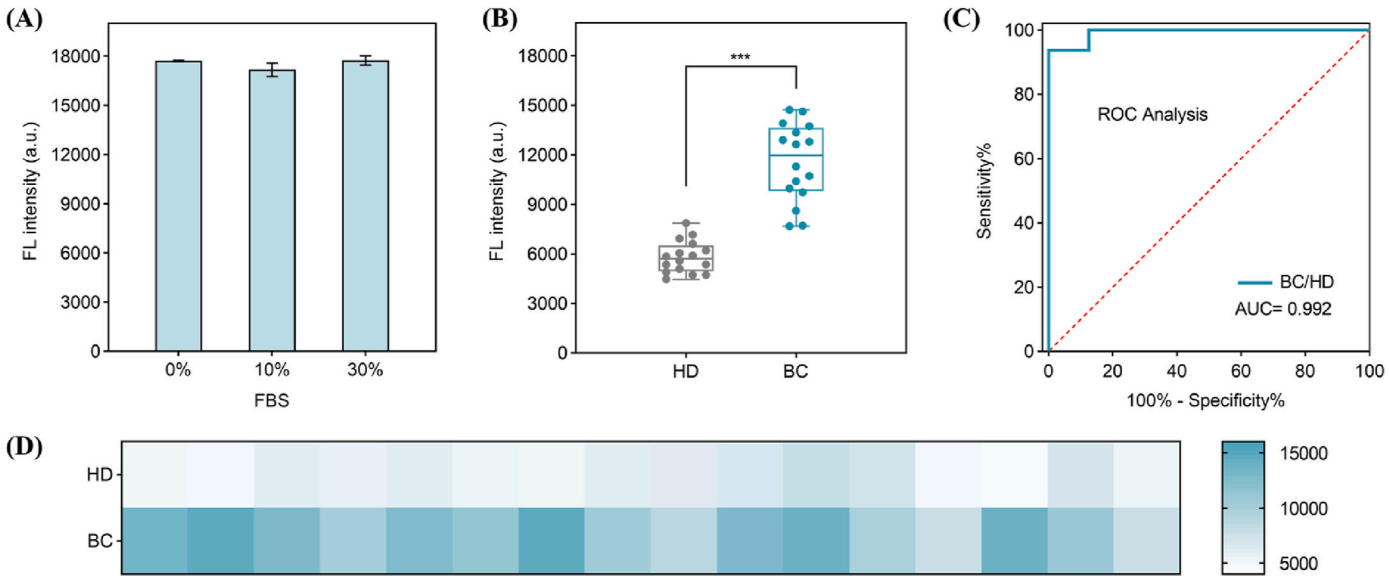



**Fig. 6.** (A) The detection of sEVs ($1.7 \times 10^7$ particles/mL) in complex samples (0 %, 10 % and 30 % FBS). AND logic gate-driven Alt-PER-Cas12a sensing platform for distinguishing breast cancer (BC) patients from healthy donors (HD). The fluorescence intensity of (B) scatter box plot, (C) ROC analysis plot, and (D) Heatmap.

Supervision, Funding acquisition, Conceptualization. **Yuezhong Xian:** Writing – review & editing, Supervision, Funding acquisition.

## Declaration of competing interest

The authors declare that they have no known competing financial interests or personal relationships that could have appeared to influence the work reported in this paper.

## Acknowledgments

The authors gratefully thank Associate Prof. Hui Shi from the Institute of Stem Cell, School of Medicine, Jiangsu University, for sharing the clinical samples. This work was supported by the National Natural Science Foundation of China (22274054, 21974050), Shanghai Magnolia Talent Plan Pujiang Project (24PJD027), and Natural Science Foundation of Shanghai (20ZR1418000).

## Appendix A. Supplementary data

Supplementary data to this article can be found online at https://doi.org/10.1016/j.talanta.2025.128411.

## Data availability

Data will be made available on request.

## References

[1] F. Bray, M. Laversanne, H.Y.A. Sung, J. Ferlay, R.L. Siegel, I. Soerjomataram, A. Jemal, Global cancer statistics 2022: GLOBOCAN estimates of incidence and mortality worldwide for 36 cancers in 185 countries, Ca-Cancer J. Clin. 74 (2024) 229–263, https://doi.org/10.3322/caac.21834.

[2] A.M. Filho, M. Laversanne, J. Ferlay, M. Colombet, M. Pineros, A. Znaor, D. M. Parkin, I. Soerjomataram, F. Bray, The GLOBOCAN 2022 cancer estimates: data sources, methods, and a snapshot of the cancer burden worldwide, Int. J. Cancer 156 (2025) 1336–1346, https://doi.org/10.1002/ijc.35278.

[3] A.N. Giaquinto, H. Sung, L.A. Newman, R.A. Freedman, R.A. Smith, J. Star, A. Jemal, R.L. Siegel, Breast cancer statistics 2024, Ca-Cancer J. Clin. 74 (2024) 477–495, https://doi.org/10.3322/caac.21863.

[4] R.L. Siegel, K.D. Miller, N.S. Wagle, A. Jemal, Cancer statistics, Ca-Cancer J. Clin. 73 (2023) 17–48, https://doi.org/10.3322/caac.21763, 2023.

[5] F. Brasó-Maristany, G. Griguolo, T. Pascual, L. Paré, P. Nuciforo, A. Llombart-Cussac, B. Bermejo, M. Oliveira, S. Morales, N. Martínez, M. Vidal, B. Adamo, O. Martínez, S. Pernas, R. López, M. Muñoz, N. Chic, P. Galván, I. Garau, L. Manso, J. Alarcón, E. Martínez, S. Gregorio, R.R. Gomis, P. Villagrasa, J. Cortés, E. Ciruelos, A. Prat, Phenotypic changes of HER2-positive breast cancer during and after dual HER2 blockade, Nat. Commun. 11 (2020) 385, https://doi.org/10.1038/s41467-019-14111-3.

[6] Z.Y. He, Z. Chen, M.D. Tan, S. Elingarami, Y. Liu, T.T. Li, Y. Deng, N.Y. He, S. Li, J. Fu, W. Li, A review on methods for diagnosis of breast cancer cells and tissues, Cell Prolif. 53 (2020) e12822, https://doi.org/10.1111/cpr.12822.

[7] S.H. Jafari, Z. Saadatpour, A. Salmaninejad, F. Momeni, M. Mokhtari, J.S. Nahand, M. Rahmati, H. Mirzaei, M. Kianmehr, Breast cancer diagnosis: imaging techniques and biochemical markers, J. Cell. Physiol. 233 (2018) 5200–5213, https://doi.org/10.1002/jcp.26379.

[8] R. Vaidyanathan, R.H. Soon, P. Zhang, K. Jiang, C.T. Lim, Cancer diagnosis: from tumor to liquid biopsy and beyond, Lab Chip 19 (2019) 11–34, https://doi.org/10.1039/c8lc00684a.

[9] S.C. Baca, J.H. Seo, M.P. Davidsohn, B. Fortunato, K. Semaan, S. Sotudian, G. Lakshminarayanan, M. Diossy, X.T. Qiu, T. El Zarif, H. Savignano, J. Canniff, I. Madueke, R.M. Saliby, Z.W. Zhang, R. Li, Y.J. Jiang, L. Taing, M. Awad, C. H. Chau, J.A. Decaprio, W.D. Figg, T.F. Greten, A.N. Hata, F.S. Hodi, M.E. Hughes, K.L. Ligon, N.Y. Lin, K. Ng, M.G. Oser, C. Meador, H.A. Parsons, M.M. Pomerantz, A. Rajan, J. Ritz, M. Thakuria, S.M. Tolaney, P.Y. Wen, H.Y. Long, J.E. Berchuck, Z. Szallasi, T.K. Choueiri, M.L. Freedman, Liquid biopsy epigenomic profiling for cancer subtyping, Nat. Med. 29 (2023) 2737–2741, https://doi.org/10.1038/s41591-023-02605-z.

[10] M. Ignatiadis, G.W. Sledge, S.S. Jeffrey, Liquid biopsy enters the clinic - implementation issues and future challenges, Nat. Rev. Clin. Oncol. 18 (2021) 297–312, https://doi.org/10.1038/s41571-020-00457-x.

[11] R. Kalluri, V.S. LeBleu, The biology, function, and biomedical applications of exosomes, Science 367 (2020) eaau6977, https://doi.org/10.1126/science.aau6977.

[12] H.L. Shao, H. Im, C.M. Castro, X. Breakefield, R. Weissleder, H.H. Lee, New technologies for analysis of extracellular vesicles, Chem. Rev. 118 (2018) 1917–1950, https://doi.org/10.1021/acs.chemrev.7b00534.

[13] M. Lu, W. Shao, H. Xing, Y. Huang, Extracellular vesicle-based nucleic acid delivery, Interdisciplinary Medicine 1 (2023) e20220007, https://doi.org/10.1002/inmd.20220007.

[14] L. Zhang, D.H. Yu, Exosomes in cancer development, metastasis, and immunity, Biochimica et Biophysica Acta (BBA)-Reviews on Cancer 1871 (2019) 455–468, https://doi.org/10.1016/j.bbcan.2019.04.004.

[15] T.B. Steinbichler, J. Dudás, H. Riechelmann, I.I. Skvortsova, The role of exosomes in cancer metastasis, Semin. Cancer Biol. 44 (2017) 170–181, https://doi.org/10.1016/j.semcancer.2017.02.006.

[16] X. Wang, L. Tian, J.Y. Lu, I.O.L. Ng, Exosomes and cancer-diagnostic and prognostic biomarkers and therapeutic vehicle, Oncogenesis 11 (2022) 54, https://doi.org/10.1038/s41389-022-00431-5.

[17] Y. Cao, X.M. Yu, T.Y. Zeng, Z.Y. Fu, Y.Y. Zhao, B.B. Nie, J. Zhao, Y.M. Yin, G.X. Li, Molecular characterization of exosomes for subtype-based diagnosis of breast cancer, J. Am. Chem. Soc. 144 (2022) 13475–13486, https://doi.org/10.1021/jacs.2c00119.

[18] W.Y. Sun, Y. Wang, Z.X. Zhu, Y.R. Wang, M.R. Zhang, L. Jiang, S. Liu, J.H. Yu, J. D. Huang, Accurate and nonpurified identification of extracellular vesicles using dual-binding recognition mode, Anal. Chem. 93 (2021) 12383–12390, https://doi.org/10.1021/acs.analchem.1c02259.

[19] W.Q. Tan, C.L. Zhang, S.S. Cheng, X.Y. Hu, M. Wang, Y.Z. Xian, DNA gate-based CRISPR-Cas exponential amplification system for ultrasensitive small extracellular

vesicle detection to enhance breast cancer diagnosis, Anal. Chem. 96 (2024) 1328–1335, https://doi.org/10.1021/acs.analchem.3c04873.
[20] Y. Cao, Y. Wang, X. Yu, X. Jiang, G. Li, J. Zhao, Identification of programmed death ligand-1 positive exosomes in breast cancer based on DNA amplification-responsive metal-organic frameworks, Biosens. Bioelectron. 166 (2020) 112452, https://doi.org/10.1016/j.bios.2020.112452.
[21] X. Gao, X. Teng, Y. Dai, J. Li, Rolling circle amplification-assisted flow cytometry approach for simultaneous profiling of exosomal surface proteins, ACS Sens. 6 (2021) 3611–3620, https://doi.org/10.1021/acssensors.1c01163.
[22] X.Y. Li, Y.J. Liu, Y.P. Fan, G. Tian, B. Shen, S.Z. Zhang, X.H. Fu, W. He, X.Y. Tao, X. J. Ding, X.M. Li, S.J. Ding, Advanced nanoencapsulation-enabled ultrasensitive analysis: unraveling tumor extracellular vesicle subpopulations for differential diagnosis of hepatocellular carcinoma via dna cascade reactions, ACS Nano 18 (2024) 11389–11403, https://doi.org/10.1021/acsnano.4c01310.
[23] X.Y. Li, X.M. Li, X.X. Cheng, X.T. Bian, B. Shen, X.J. Ding, S.J. Ding, Single-step and highly sensitive imaging of exosomal pd-l1 through aptamer-activated cascade primer exchange reaction-generated branched dna nanostructures, ACS Sens. 7 (2022) 3571–3579, https://doi.org/10.1021/acssensors.2c01614.
[24] L. Hu, W. Chen, S. Zhou, G. Zhu, ExoHCR: a sensitive assay to profile PD-L1 level on tumor exosomes for immunotherapeutic prognosis, Biophysics Reports 6 (2020) 290–298, https://doi.org/10.1007/s41048-020-00122-x.
[25] M. Ye, Q. Niu, L. Yan, J. Feng, L. Wu, X. Hu, Q. Xu, Y. Shu, Paper-based lipid bilayer magnetic interface for ultrasensitive assay of tumor-derived extracellular vesicles PD-L1, Sensors and Actuators B Chemical 399 (2024) 134819, https://doi.org/10.1016/j.snb.2023.134819.
[26] S.S. Cheng, Q.Q. Kong, X.Y. Hu, C.L. Zhang, Y.Z. Xian, An ultrasensitive strand displacement signal amplification-assisted synchronous fluorescence assay for surface proteins of small extracellular vesicle analysis and cancer identification, Anal. Chem. 94 (2022) 1085–1091, https://doi.org/10.1021/acs.analchem.1c04122.
[27] S. Xing, Z. Lu, Q. Huang, H. Li, Y. Wang, Y. Lai, Y. He, M. Deng, W. Liu, An ultrasensitive hybridization chain reaction-amplified CRISPR-Cas12a aptasensor for extracellular vesicle surface protein quantification, Theranostics 10 (2020) 10262–10273, https://doi.org/10.7150/thno.49047.
[28] J.Y. Kishi, T.E. Schaus, N. Gopalkrishnan, F. Xuan, P. Yin, Programmable autonomous synthesis of single-stranded DNA, Nat. Chem. 10 (2018) 155–164, https://doi.org/10.1038/nchem.2872.
[29] D.D. Wang, J. Zhang, Q.Q. Yu, K. Zhang, T.T. Chen, X. Chu, Biomineralized zeolitic imidazolate framework-8 nanoparticles enable polymerase-driven DNA biocomputing for reliable cell identification, Anal. Chem. 94 (2022) 4794–4802, https://doi.org/10.1021/acs.analchem.1c05605.
[30] Q. Zhang, R. Zhao, Y. Zhang, X.R. Zou, C.Y. Zhang, One-step self-assembly of quantum dot-based spherical nucleic acid nanostructure for accurate monitoring of long noncoding RNA MALAT1 in living cells and tissues, Chemical Engineering Journal 469 (2023) 144021, https://doi.org/10.1016/j.cej.2023.144021.
[31] Y.M. Lai, W. Xiao, Z.W. Lei, H.P. Long, J.T. Deng, Y.Y. Wang, L. Tao, X.X. Liu, J. J. Wu, Q.W. Zhang, D.L. Cao, H. Xiao, Primer exchange reaction with cascade RNA transcription for highly specific detection of exosomal miRNA and liver cancer diagnosis, Anal. Chem. 97 (2025) 4151–4157, https://doi.org/10.1021/acs.analchem.4c06517.
[32] Z.P. Wang, A.M. Ma, Y.P. Chen, An amplification-free digital assay based on primer exchange reaction-mediated botryoidal-like fluorescent polystyrene dots to detect multiple pathogenic bacteria, ACS Nano 18 (2024) 31174–31187, https://doi.org/10.1021/acsnano.4c09069.
[33] J.L. Zhang, M.T. Guan, M. Lv, Y.Y. Liu, H.L. Zhang, Z.Z. Zhang, K.X. Zhang, Localized imaging of programmed death-ligand 1 on individual tumor-derived extracellular vesicles for prediction of immunotherapy response, ACS Nano 17 (2023) 20120–20134, https://doi.org/10.1021/acsnano.3c05799.
[34] S.K. Saka, Y. Wang, J.Y. Kishi, A. Zhu, Y.T. Zeng, W.X. Xie, K. Kirli, C. Yapp, M. Cicconet, B.J. Beliveau, S.W. Lapan, S.Y. Yin, M. Lin, E.S. Boyden, P.S. Kaeser, G. Pihan, G.M. Church, P. Yin, Immuno-SABER enables highly multiplexed and amplified protein imaging in tissues, Nat. Biotechnol. 37 (2019) 1080–1090, https://doi.org/10.1038/s41587-019-0207-y.
[35] X.Y. Hu, S.S. Cheng, X.Z. Luo, Y.Z. Xian, C.L. Zhang, Polymerase-driven logic signal amplification for the detection of small extracellular vesicle surface proteins and the identification of breast cancer, Anal. Chem. 95 (2023) 10330–10336, https://doi.org/10.1021/acs.analchem.3c01080.
[36] E. Ma, K. Chen, H.L. Shi, E.C. Stahl, B. Adler, M. Trinidad, J.J. Liu, K.H. Zhou, J. J. Ye, J.A. Doudna, Improved genome editing by an engineered CRISPR-Cas12a, Nucleic Acids Res. 50 (2022) 12689–12701, https://doi.org/10.1093/nar/gkac1192.
[37] Z.Y. Weng, Z. You, J. Yang, N. Mohammad, M.S. Lin, Q.S. Wei, X. Gao, Y. Zhang, CRISPR-Cas biochemistry and CRISPR-based molecular diagnostics, Angew. Chem. Int. Ed. 62 (2023) e202214987, https://doi.org/10.1002/anie.202214987.
[38] W. Tang, J. Liu, B. Ding, Nucleic acid nanostructure for delivery of CRISPR/Cas9-based gene editing system, Interdisciplinary Medicine 1 (2023) e20220014, https://doi.org/10.1002/inmd.20220014.
[39] J.S. Chen, E.B. Ma, L.B. Harrington, M. Da Costa, X.R. Tian, J.M. Palefsky, J. A. Doudna, CRISPR-Cas12a target binding unleashes indiscriminate single-stranded DNase activity, Science 360 (2018) 436–439, https://doi.org/10.1126/science.aar6245.
[40] S.Y. Li, Q.X. Cheng, J.K. Liu, X.Q. Nie, G.P. Zhao, J. Wang, CRISPR-Cas12a has both cis- and trans-cleavage activities on single-stranded DNA, Cell Res. 28 (2018) 491–493, https://doi.org/10.1038/s41422-018-0022-x.
[41] J.P.K. Bravo, T. Hallmark, B. Naegle, C.L. Beisel, R.N. Jackson, D.W. Taylor, RNA targeting unleashes indiscriminate nuclease activity of CRISPR-Cas12a2, Nature 613 (2023) 582–587, https://doi.org/10.1038/s41586-022-05560-w.
[42] H. Yue, M. Huang, T. Tian, E. Xiong, X. Zhou, Advances in clustered, regularly interspaced short palindromic repeats (CRISPR)-based diagnostic assays assisted by micro/nanotechnologies, ACS Nano 15 (2021) 7848–7859, https://doi.org/10.1021/acsnano.1c02372.
[43] Y. Xiong, J.J. Zhang, Z.L. Yang, Q.B. Mou, Y. Ma, Y.H. Xiong, Y. Lu, Functional DNA regulated CRISPR-Cas12a sensors for point-of-care diagnostics of non-nucleic-acid targets, J. Am. Chem. Soc. 142 (2020) 207–213, https://doi.org/10.1021/jacs.9b09211.
[44] S.R. Rananaware, E.K. Vesco, G.M. Shoemaker, S.S. Anekar, L.S.W. Sandoval, K. S. Meister, N.C. Macaluso, L.T. Nguyen, P.K. Jain, Programmable RNA detection with CRISPR-Cas12a, Nat. Commun. 14 (2023) 5409, https://doi.org/10.1038/s41467-023-41006-1.
[45] D. Samanta, S.B. Ebrahimi, N. Ramani, C.A. Mirkin, Enhancing CRISPR-Cas-mediated detection of nucleic acid and non-nucleic acid targets using enzyme-labeled reporters, J. Am. Chem. Soc. 144 (2022) 16310–16315, https://doi.org/10.1021/jacs.2c07625.
[46] B.M. Youngquist, J. Saliba, Y. Kim, T.J. Cutro, C.J. Lyon, J. Olivo, N. Ha, J. Fine, R. Colman, C. Vergara, J. Robinson, S. Lacourse, R.S. Garfein, D.G. Catanzaro, C. Lange, E. Perez-Then, E.A. Graviss, C.D. Mitchell, T. Rodwell, B. Ning, T.Y. Hu, Rapid tuberculosis diagnosis from respiratory or blood samples by a low cost, portable lab-in-tube assay, Sci. Transl. Med. 17 (2025) eadp6411, https://doi.org/10.1126/scitranslmed.adp6411.
[47] R. Li, Y. Zhu, X. Gong, Y. Zhang, C. Hong, Y. Wan, X. Liu, F. Wang, Self-stacking autocatalytic molecular circuit with minimal catalytic DNA assembly, J. Am. Chem. Soc. 145 (2023) 2999–3007, https://doi.org/10.1021/jacs.2c11504.
[48] H. Yan, Y. Wen, Z. Tian, N. Hart, S. Han, S.J. Hughes, Y. Zeng, A one-pot isothermal Cas12-based assay for the sensitive detection of microRNAs, Nat. Biomed. Eng. 7 (2023) 1583–1601, https://doi.org/10.1038/s41551-023-01033-1.
[49] X. Gu, J. Zhang, J. Liang, X. Liu, X. He, X. Jin, C. Yan, L. Wang, C. Song, CRISPR/Cas13a trans-cleavage and catalytic hairpin assembly cascaded signal amplification powered SERS aptasensor for ultrasensitive detection of gastric cancer-derived exosomes, Anal. Chem. 96 (2024) 18681–18689, https://doi.org/10.1021/acs.analchem.4c03063.
[50] S. Zhou, T. Hu, F. Zhang, D. Tang, D. Li, J. Cao, W. Wei, Y. Wu, S. Liu, Integrated microfluidic device for accurate extracellular vesicle quantification and protein markers analysis directly from human whole blood, Anal. Chem. 92 (2020) 1574–1581, https://doi.org/10.1021/acs.analchem.9b04852.
[51] J. Zhang, J. Shi, H. Zhang, Y. Zhu, W. Liu, K. Zhang, Z. Zhang, Localized fluorescent imaging of multiple proteins on individual extracellular vesicles using rolling circle amplification for cancer diagnosis, J. Extracell. Vesicles 10 (2020) e12025, https://doi.org/10.1002/jev2.12025.
[52] J.Q. Deng, S. Zhao, J.H. Li, Y.C. Cheng, C. Liu, Z. Liu, L.L. Li, F. Tian, B. Dai, J. S. Sun, One-step thermophoretic AND gate operation on extracellular vesicles improves diagnosis of prostate cancer, Angew. Chem. Int. Ed. 61 (2022) e202207037, https://doi.org/10.1002/anie.202207037.
[53] J.Q. Liu, Z.D. Liu, C.Q. Zhao, Y.T. Jiao, B.H. Li, J.J. Shi, Z.C. Chen, Z. Zhang, Coaxial dual-path electrochemical biosensing and logic strategy-based detection of lung cancer-derived exosomal PD-L1, Nanoscale 16 (2024) 8950–8959, https://doi.org/10.1039/d4nr00412d.
[54] Y. Feng, Y. Yang, P. Guo, L. Zhang, Y. Yang, Z. Zhao, C. Cui, Q. Yang, Y. Liu, L. Yang, R. Peng, W. Tan, DNA self-assembly generated by aptamer-triggered rolling circle amplification cascades for profiling colorectal cancer-derived small extracellular vesicles, ACS Nano 19 (2025) 2294–2305, https://doi.org/10.1021/acsnano.4c12286.
[55] Q. Wu, Q. Wu, H. Lin, C. Zhang, Z. You, S. Kang, Y. Xu, X. Chen, C. Yang, Y. Song, L. Zhu, Microfluidic replication and phenotypic profiling of extracellular vesicles from the tumor microenvironment using dual-switch aptamer logic gates, Anal. Chem. 97 (2025) 5313–5323, https://doi.org/10.1021/acs.analchem.5c00234.
[56] L.M. Yang, J.G. Zhang, J. Zhang, T. Hou, Q. Gao, X.J. Liu, F. Li, CRISPR-based homogeneous electrochemical strategy for near-zero background detection of breast cancer extracellular vesicles via fluidity-enhanced magnetic capture nanoprobe, Anal. Chem. 97 (2025) 2176–2185, https://doi.org/10.1021/acs.analchem.4c05181.
[57] M.Z. Zhao, Q. Li, Y. Zhao, H.L. Zhou, Y.T. Yan, R.M. Kong, Q.Q. Tan, W.H. Kong, F. L. Qu, Dual-aptamer recognition of DNA logic gate sensor-based specific exosomal proteins for ovarian cancer diagnosis, ACS Sens. 9 (2024) 2540–2549, https://doi.org/10.1021/acssensors.4c00270.
[58] L.L. Wu, Y.D. Wang, X. Xu, Y.L. Liu, B.Q. Lin, M.X. Zhang, J.L. Zhang, S. Wan, C. Y. Yang, W.H. Tan, Aptamer-based detection of circulating targets for precision medicine, Chem. Rev. 121 (2021) 12035–12105, https://doi.org/10.1021/acs.chemrev.0c01140.
[59] J.Q. Deng, C. Liu, J.S. Sun, DNA-based nanomaterials for analysis of extracellular vesicles, Adv. Mater. 36 (2024) 2303092, https://doi.org/10.1002/adma.202303092.
[60] Y. Zhu, W. Li, F. Lan, S. Chen, X. Chen, X. Zhang, X. Yan, Y. Zhang, DNA nanotechnology in tumor liquid biopsy: enrichment and determination of circulating biomarkers, Interdisciplinary Medicine 2 (2024) e20230043, https://doi.org/10.1002/inmd.20230043.
[61] T.A. Feagin, N. Maganzini, H.T. Soh, Strategies for creating structure-switching aptamers, ACS Sens. 3 (2018) 1611–1615, https://doi.org/10.1021/acssensors.8b00516.
[62] L. Li, X.G. Chen, C. Cui, X.S. Pan, X.W. Li, H.S. Yazd, Q. Wu, L.P. Qiu, J. Li, W. H. Tan, Aptamer displacement reaction from live-cell surfaces and its applications,

J. Am. Chem. Soc. 141 (2019) 17174–17179, https://doi.org/10.1021/jacs.9b07191.
[63] R. Nutiu, Y.F. Li, Structure-switching signaling aptamers, J. Am. Chem. Soc. 125 (2003) 4771–4778, https://doi.org/10.1021/ja028962o.
[64] B.D. Wilson, A.A. Hariri, I.A.P. Thompson, M. Eisenstein, H.T. Soh, Independent control of the thermodynamic and kinetic properties of aptamer switches, Nat. Commun. 10 (2019) 5079, https://doi.org/10.1038/s41467-019-13137-x.
[65] A.M. Yoshikawa, A.E. Rangel, L.W. Zheng, L.G. Wan, L.A. Hein, A.A. Hariri, M. Eisenstein, H.T. Soh, A massively parallel screening platform for converting aptamers into molecular switches, Nat. Commun. 14 (2023) 2336, https://doi.org/10.1038/s41467-023-38105-4.